Characterization of solidification and hot workability of MgAl6Mn foundry alloy

Primož Mrvar, Milan Terčelj, Goran Kugler,
Matevž Fazarinc and Jožef Medved

University of Ljubljana; Faculty of Natural Sciences and Engineering,
Department of Materials and Metallurgy, Aškerčeva cesta 12, 1000 Ljubljana, Slovenia;
E-mail: primoz.mrvar@ntf.uni-lj.si, milan.tercelj@ntf.uni-lj.si,
goran.kugler@ntf.uni-lj.si, jozef.medved@ntf.uni-lj.si

Received: September 11, 2006 **Accepted**: October 20, 2006

Abstract: Solidification at cooling rate 7 K/min and hot workability of MgAl6Mn (AM60) alloy have been studied. Metallographic examinations, simultaneous thermal analyses (STA) and thermodynamic calculations are also included in the contribution. The following characteristic temperatures of the solidification process have been established from the cooling curves and STA curves: the liquidus temperature T_L, solidus T_S, and eutectic temperature T_E, respectively. The $Mg_{17}Al_{12}$ phase and eutectic ($\alpha_{Mg} + Mg_{17}Al_{12}$), which precipitated on the boundaries of the primary α_{Mg} grains, are observed in MgAl6Mn alloy. It is caused by the local Al – micro segregations in last solidified areas. In MgAl6Mn alloy also formation of the Al_4Mn inter-metallic compound occurred. The consequence of that is the decreased concentration of the dissolved Al in the Mg-Al liquid solution. Further, the deformation behavior of as-cast MgAl6Mn alloy in the temperature range 200-450 °C and in the strain rate range 0.001-10 $^{s-1}$ has been studied using processing maps. Upper (400-450 °C) and lower (200-250 °C) temperature regions and higher strain rates (5, 10 $^{s-1}$) are not appropriate for hot forming due to cracking on grain boundaries. The mean reason for cracking in lower temperature range (200-250 °C) cracking is presence of $Mg_{17}Al_{12}$ inter-metallic phase and ($\alpha_{Mg} + Al_{12}Mg_{17}$) un-equilibrium eutectic. In upper temperature range (400-450 °C) the melting of ($\alpha_{Mg} + Al_{12}Mg_{17}$) eutectic at 426 °C is responsible for grain boundary cracking. Calculated activation energy Q for researched alloy amounts 160.5 kJ mol^{-1}.

Key words: MgAl6Mn alloy, solidification process, inter-metallic compounds, as-cast state, hot forming

Introduction

The use of the up-to date light alloys and their development are in the sharp ascent especially in transportation industry since in the last years the use of the magnesium alloys for the various purposes was strongly increased. The advantages of the magnesium alloys are in its little weight of the final products, good machinability, corrosion resistance and good mechanical properties. Thus they can compete with aluminium alloys and even steels. Due to the high prices of the basic material and difficulties on the technological melting, on casting and on hot working processes of the magnesium alloys, the thermodynamically investigations of the solidification and of hot working are needed for better knowl-

Scientific paper

edge and optimisation of all technological processes. Magnesium alloys are based upon the binary diagram of Mg-Al and it contain from 2 to 9 mass. % Al[1]. Decreased hot formability of Mg alloys originates from their hexagonal close-packed structure. MgAl6Mn (AM60) alloy is predominately used for casting and its product have found application in the aircraft parts, car parts, etc.; but its application could be increased if the mechanical properties (tensile strength, ductility, hardness, etc.) will be improved. It is well known that deformed microstructure posses higher mechanical properties in comparison to as-cast state and that the homogenisation process is needed before hot forming; mentioned homogenization process thus increases the production costs.

Thus the aim of this research was to study the solidification and the possibility of hot working of AM60 foundry alloy without prior homogenisation process. The solidification of gravity cast magnesium alloy AM60 has been investigated with the various methods of the thermal analysis: "in situ" simple thermal analysis and simultaneous thermal analysis. The experimental results were upgraded with the thermodynamic calculation and the results of the metallographic analysis. Further the deformation behavior of as-cast MgAl6Mn alloy in the temperature range 200-450 °C and in the strain rate range 0.001-10 s^{-1} using processing maps has been studied in order to reveal optimal hot working conditions.

CASTING - EXPERIMENTAL PROCEDURE AND RESULTS

Casting proceeding, specimens and material

The investigated alloy was prepared by the re-melting of the standard MgAl6Mn (AM60) alloy what was done in the graphite crucible of the inductive furnace. In Table 1 the chemical composition of the MgAl6Mn alloy and the fraction of the each element is presented. The melting was taking place under the protective atmosphere of argon. When the temperature of 720 °C was achieved the melt from the graphite crucible was cast into measuring cells Figure 1a, and the cooling curves were measured. Thermal analysis was taking place in simple thermal

a.)

b.)

Figure 1. Equipment with the measuring cell for "in situ" thermal analyses.

Table 1. Chemical composition of MgAl6Mn alloy and according to the standard EN 1753

Element	AM60 [mass.%]	Sample [mass.%]
Al	5,8-6,40	6,28
Zn	<0,20	0,1267
Mn	>0,3	0,3056
Cu	<0,008	0,005
Si	<0,05	0,0294
Fe	<0,004	0,0032
Ni	<0,001	<0,0008
Mg	remain	93,2

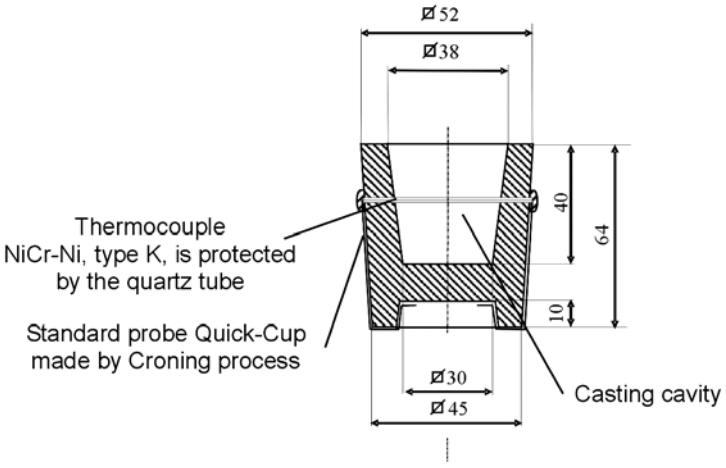

Figure 2. Detailer presentation of the measuring cell for "in situ" simple thermal analyses and samples for further investigations.

analyses called ETA1.2[2-3] (Figures 1 and 2). In Figure 1a the measuring cell with holder and in Figure 1b the measuring system are presented, respectively.

The thermal analysis of MgAl6Mn alloy (dimensions ϕ=5 mm x 4 mm) has been investigated by the STA 449 Jupiter (Netzsch) apparatus (nitrogen protective atmosphere). The samples were heated to the temperature of 720 °C by the rate of 7 K/min, and then were cooled by the same rate to the room temperature.

Thermodinamical calculation

Thermodynamical calculation (Figure 3) was made by the Thermo-Calc software according to the chemical composition given in Table 1. All the equilibrium phases and their temperature range of stability had been calculated. At 632 °C phase Al_8Mn_5 precipitate from liquid and then at temperature 617 °C the primary crystals of aMg form and start to grow. The inter-metallic compound Mg_2Si also precipitates at temperature 538 °C. Inter-metallic compound Al_8Mn_5 transform into $Al_{11}Mn_4$ and later it will be transformed into the inter-metallic compound Al Mn. In

coordinate with phase diagram presented on Figure 3 at temperature of crossing the solvus line (287 °C) the $Mg_{17}Al_{12}$ inter-metallic compound start to precipitate from α_{Mg}. At room temperature microstructure is form from solid solution of α_{Mg} and inter-metallic compounds Al_4Mn and $Mg_{17}Al_{12}$.

Simultaneous thermal analyses

With apparatus for simultaneous thermal analyses (STA) the MgAl6Mn alloy was analysed. The results in form of heating and cooling curves are presented in Figure 4 and 5, respectively. At heating process (Figure 4)

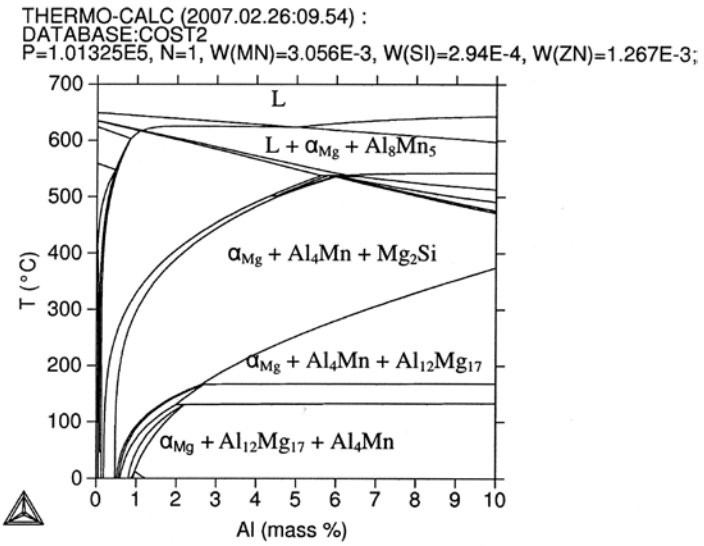

Figure 3. Isopleth phase diagram Mg - Al - Mn at 0.3056 mass. % manganese, THERMOCALC

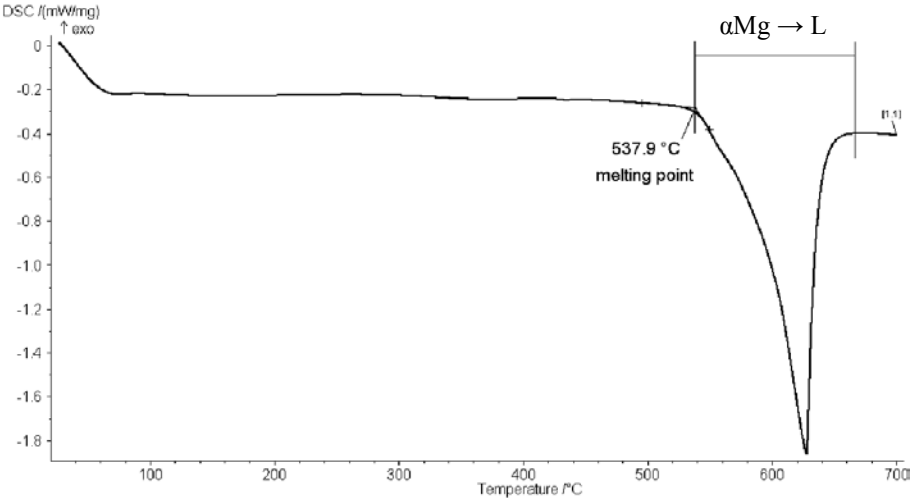

Figure 4. STA heating curve of the AM60 alloy in the as-cast state

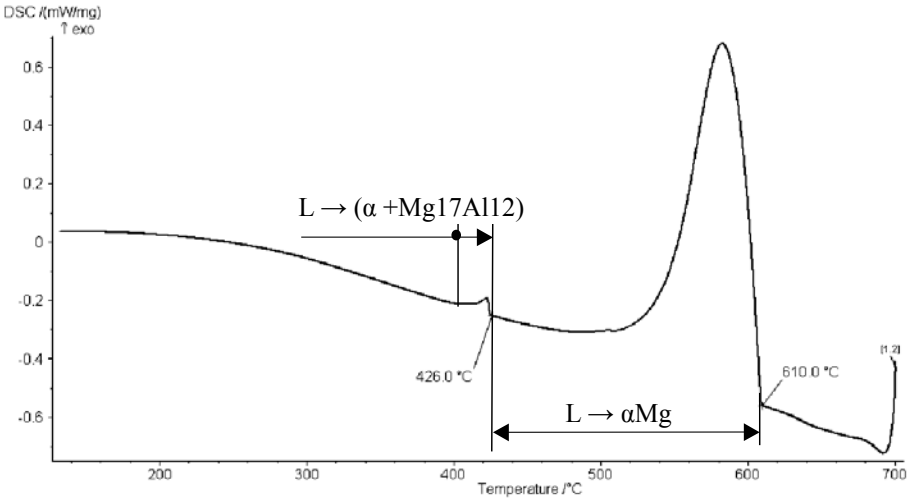

Figure 5. STA cooling curve of the AM60 alloy

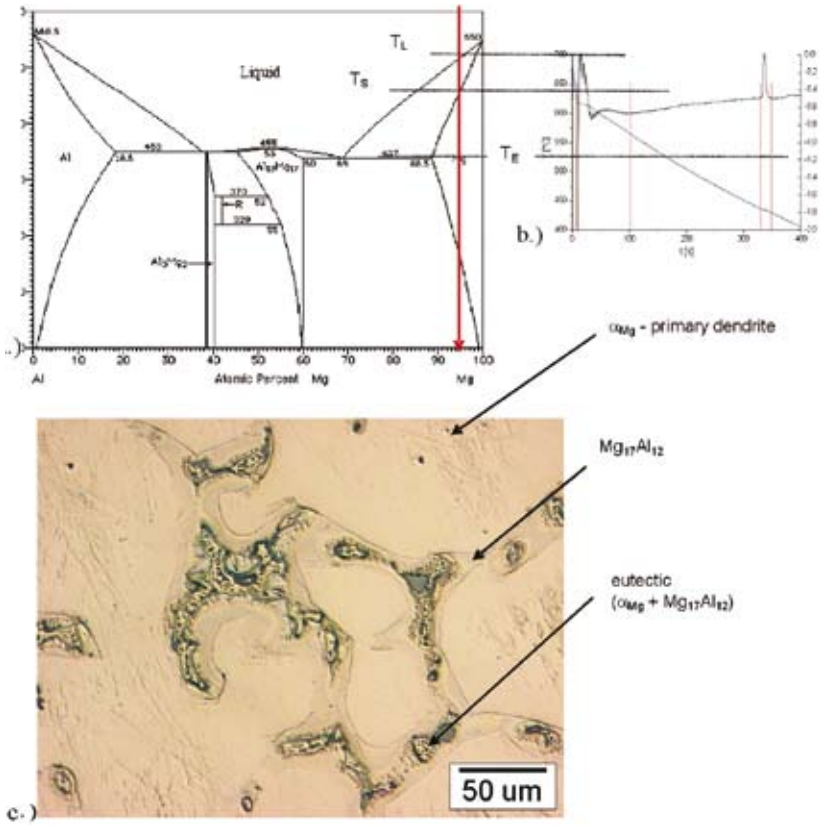

Figure 6. Solidification of AM60 alloy at low cooling rate, a.) binary phase diagram, b.) cooling curve, c.) microstructure of AM60 (as-casted state) at solidification rate 7 K/min

the melting start at solidus temperature (T_S), which is detected at 537.9 °C. From STA liquidus temperature could be determined from cooling curve which is detected at 610 °C (Figure 5). Because the local micro segregation happened during the relatively slow solidification process (cooling rate = 7 K/s) in the last solidified areas which are rich on Al, the eutectic reaction occurred ($L \rightarrow \alpha_{Mg} + Mg_{17}Al_{12}$) at 426 °C.

"In situ" simple thermal analyses and solidification process

An "In situ" simple thermal analysis (ETA) was used in order to follow the solidification process of the alloy. This way the microstructure and properties could be determined indirectly[3].

On a Figures 6a-c are clearly shown the connection between the cooling curve (Figure 6b) of the investigated sample (alloy MgAl6Mn), binary phase diagram (Figure 6a) and obtained microstructure (Figure 6c).

After the pouring of molten metal into measuring cell, the maximal temperature that was detected was cca. 700 °C (see Figure 6b). Then the cooling and contraction in liquid state follows as long as liquidus temperature (T_L) is reached. Further the solidification process occurred and finished at solidus temperature (T_S). Measured cooling rate in the centre of the measuring cell (Figure 2) was 7 K/s. Microstructure components were composed from the primary precipitated crystals of α_{Mg}. Along the boundaries of the crystal grains the eutectic ($\alpha_{Mg} + Al_{12}Mg_{17}$) has been solidified, where the local increasing of the aluminium fraction was taking places in the melt due to the aluminium segregation and therefore the eutectic solidification occurred. The reason for that is in fact that the primary solidified crystals of α_{Mg} doesn't have nominal composition of alloy X_{Al} but the concentration of Al increased and shifted left towards eutectic point (Figures 6). Formed heterogeneous eutectic is characteristically for low cooling rates. On basis of typical parameters on a cooling curve it is possible to conclude and to estimate quality of alloys.

HOT WORKING – EXPERIMENTAL PROCEDURE AND RESULTS

Equipment and experiments for hot deformation

A computer controlled servo-hydraulic machine Gleeble 1500D was used for compression testing (Figure 7). For reduction of friction between the cylindrical specimen and the tool and to avoid their mutual welding, graphite lubricant was used. Cylindrical specimens of Rastegew type with dimensions ϕ=10 mm x 15 mm (for hot compression tests) were cut from gravity cast block of dimensions 30 mm×40 mm×40 mm (see Figure 2). During testing, a stress module in the Gleeble 1500D control system calculated the instantaneous cross-sectional area of the specimen from the L-strain measurement and computed the true stress.

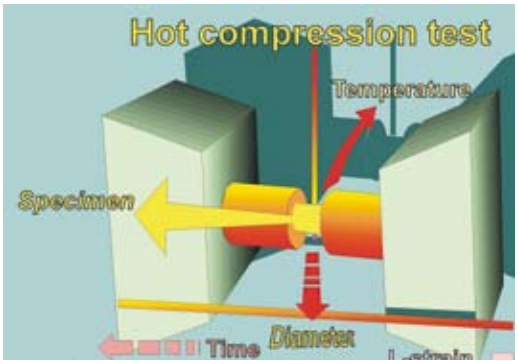

Figure 7. Schematic representation of the Gleeble compression testing arrangement

Testing was performed in the temperature range of 200 °C to 450 °C, at six different strain rates (0.001, 0.01, 0.1, 1, 5 and 10 s^{-1}). The heating rate was 3 °C/s, soaking time on deformation temperature was 15 s. After deformation the specimens were rapidly quenched with water.

On Figure 8a the flow stresses for temperature area 200 - 450 °C and strain rate 5 s^{-1} and on Figure 8b for the same temperature area but for strain rate 0.001 s^{-1} are presented. From Figure 8a is visible that hardening process occurs at samples compressed at 200 and 250 °C as a consequence of presence precipitates of $Al_{12}Mg_{17}$ inter-metallic phase and (α_{Mg} + $Al_{12}Mg_{17}$) eutectic (see Figure 9a) on grain boundaries and due to decreased activity of dynamic recovery (DRV) and recrystallization (DRX). The consequence is occurrence of cracks in/on the deformed specimen (Figure 9b).Precipitation of eutectic (α_{Mg} + $Al_{12}Mg_{17}$) begins with regards to equilibrium diagram (see Figures 3 - 6) at cca 426 °C, on the other hand the precipitation of $Al_{12}Mg_{17}$ inter-metallic compound that is more hard then α_{Mg} and thus it is from plasticity point of view undesired (in fact its precipitation begin after finished solidification process); consequently at lower temperature its fraction is still higher that additionally decreased the hot deformability. Further by decreased intensity of dynamic recovery and recrystallization at lower temperature it results in occurrence of

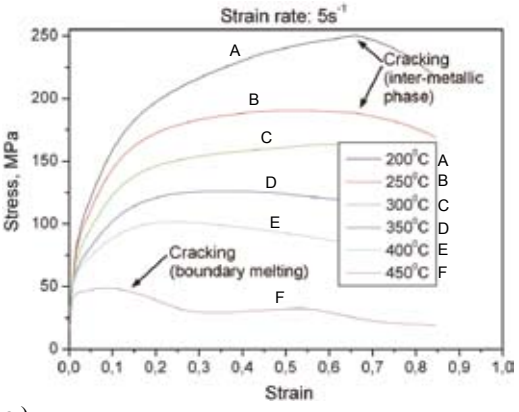

a.)

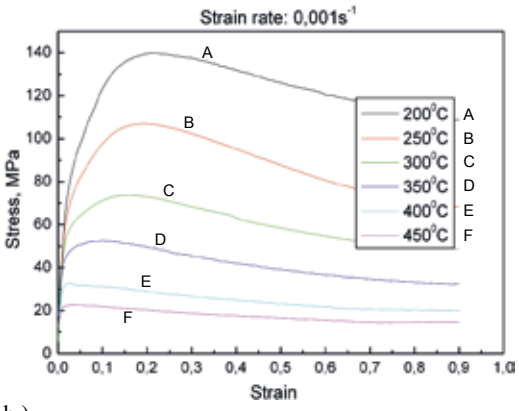

b.)

Figure 8. Flow curves, **a**-strain rate 5 s^{-1}, **b**-strain rate 0.001 s^{-1}

micro- and macro-cracks (see Figure 9b) on deformed specimen (on Figure 8a the occurrence of crack is expressed by rash change of course of flow stress). Less expressed change of flow stress course is visible at 250 °C (Figure 8a) but it also results in surface cracking of deformed specimen. The shape (course) of flow curves in temperature region 350 - 450 °C indicate the presence of dynamic recrystalization (Figure 9c); further the quick fall of flow curves occurs also at 450 °C (Figure 8a). This shape of flow stress indicates melting of precipitated phases on grain boundaries that also results in micro- and macro-cracks of the deformed specimen (Figure 9d).

At lower strain rates (0.001 - $1s^{-1}$) and at all tested temperatures after achieving of maximum the fall of flow stress is visible (Figure 8b). The density of macro-cracks obtained at higher temperatures is higher from those obtained at lower temperatures (see Figures 9b and 9d).

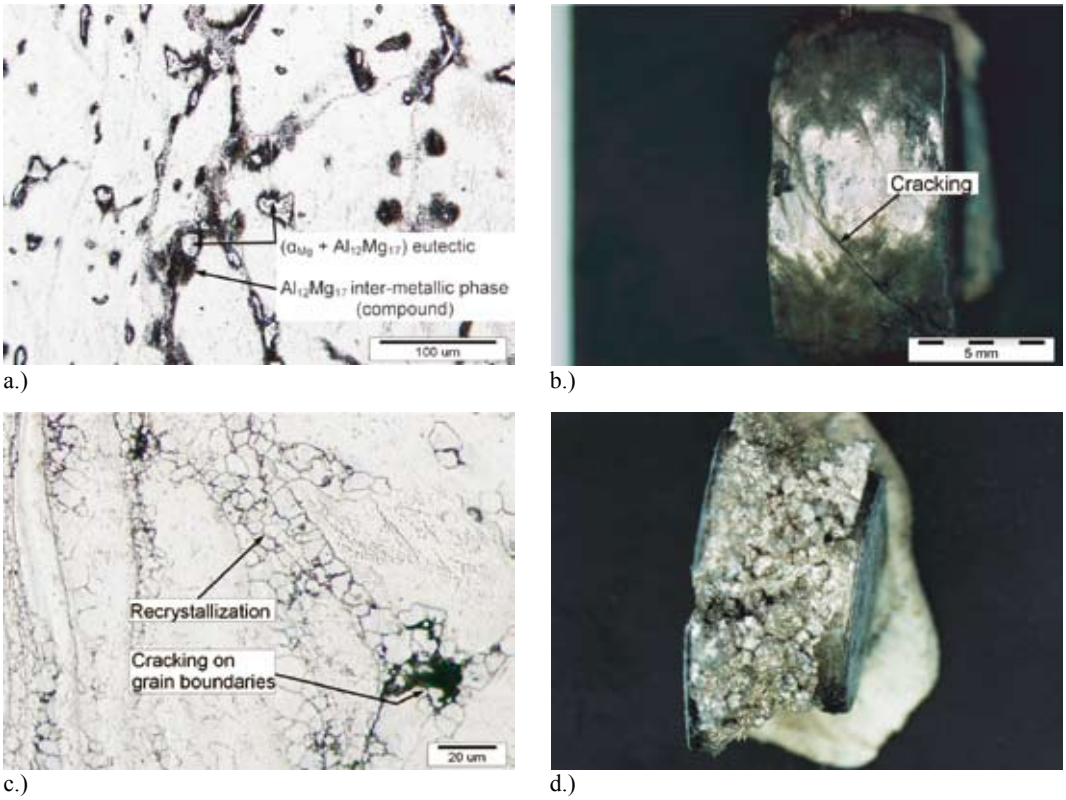

Figure 9. a-percipitation of $Al_{12}Mg_{17}$ inter-metallic phase and (α_{Mg} + $Al_{12}Mg_{17}$) eutectic on grain boundaries, **b-**crack on deformed specimen at 200 °C and strain rate 5 s^{-1}, **c-**dynamic recrystallization and **d-**cracking on grain boundaries at 450 °C and strain rate 5 s-1

Figures 10 a-b prove the presence of dynamic recrystallization at higher temperatures (350 °C).

Analytical description of flow curves

From the maximum flow stresses for different temperatures and strain rates, we calculated the constants of the hyperbolic sine equation[4-6]

$$Z = \dot{\varepsilon} \exp(Q / RT) = A(\sinh \alpha\sigma)^n \qquad (1)$$

For this purpose we first defined the function χ^2, which determines the difference between measured and calculated values of maximum flow stresses

$$\chi^2 = \sum_{i=1}^{N} \frac{(z_i - a_1 x_i - a_2 y_i - a_3)^2}{e_i^2} \qquad (2)$$

where N is the number of measurements, $z_i = \ln(\sinh\alpha\sigma_i)$, $x_i = \ln \dot{\varepsilon}_i$ and $y_i = 10^4\ T^{-1}$. Parameter $a_1 = n^{-1}$, $a_2 = 10^4\ Qn^{-1}\ R^{-1}$ and $a_3 = n^{-1} \ln A$. For the error calculation we took into account only measurement errors of the parameter z_i, given by $e_i = \alpha\ e_i^{\sigma}\ \ln(\coth\alpha\sigma_i)$, where e_i^{σ} are the measurement errors of the flow stress. The details of the minimization procedure of the above expression (2) are given elsewhere[7]. χ^2 has a minimum for Q= 160.5 kJ mol^{-1}, α=0.0216 MPa^{-1}, n=4.8 and A= 7.73·10^9 s^{-1}. For these parameters a comparison between the calculated and measured dependence of peak stress on temperature for five different strain rates is shown on Figure 11. The value for the activation energy is approximately on the level as those for aluminium[7].

a.)

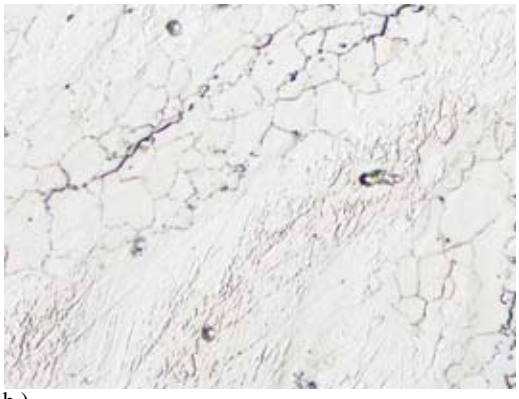

b.)

Figure 10. a-b-dynamic recrystallization in deformed specimen at 350 °C and strain rate 0.001 s^{-1}, precipitation of $Al_{12}Mg_{17}$ inter-metallic phase

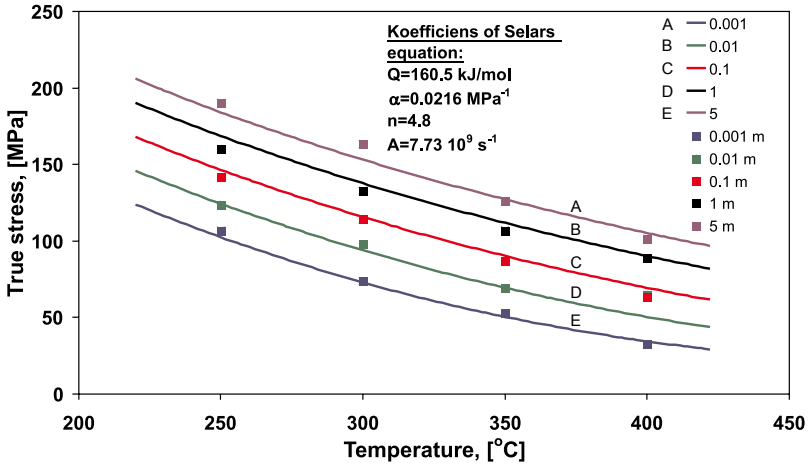

Figure 11. Comparison between measured (m) and calculated dependence of peak stress on temperature for five different strain rates of 0.001, 0.01, 0.1, 1 and 5 s^{-1}

PROCESSING MAP

Processing Map is developed on the basis of a dynamic material model (DMM) which has been developed and widely used by the group of Y. V. R. K. Prasad[8]. The Processing Map of material can be described as an explicit representation of its response to the imposed process parameters.

Efficiency of power dissipation.

The workpiece under hot deformation conditions of this model works as an essential energy dissipater. The constituent equation describes the manner in which energy (P) is converted at any instant into two forms, thermal energy (G) making temperature increase and microstructural change caused by transform of metallurgical dynamics (J), which are not recoverable. In general, most of the dissipation is due to a temperature rise and only a small amount of energy dissipates through microstructural changes. The power partitioning between G and J is controlled by the constitutive flow behavior of the material and is decided by the strain rate sensitivity (m) of flow stress as shown in the equation

$$\frac{dJ}{dG} = \frac{\dot{\varepsilon}\, d\bar{\sigma}}{\bar{\sigma}\, d\dot{\varepsilon}} = \frac{\dot{\varepsilon}\,\bar{\sigma}\, d\ln\bar{\sigma}}{\bar{\sigma}\,\dot{\varepsilon}\, d\ln\dot{\varepsilon}} \approx \frac{\Delta\log\bar{\sigma}}{\Delta\log\dot{\varepsilon}} = m \qquad (3)$$

For an ideal dissipator it can be shown that both quantities J and G are equal in their amount, which means that $m = 1$ and $J = J_{max}$ whereas the efficiency of power dissipation η is given by:

$$\eta = \frac{J}{J_{\max}} = \frac{2m}{m+1} \qquad (4)$$

The variation of η with temperature and $\dot{\varepsilon}$ represents the relative value of energy dissipation occurring through microstructural changes. Microstructural changes can be stable, which includes a dynamic recovery and dynamic recrystallization, and instable which

includes wedge cracking, void formation at hard particles, dynamic strain ageing and macrostructural cracking. As new surfaces will form during instable changes, more energy is required, while stable changes always take place by grain boundary migration.

Flow instability

The instability map is defined by a stability criterion for a dynamic material, where the differential quotient of its dissipative function has to satisfy an inequality condition, given by equation 5, to allow a stable flow.

$$\xi\left(\dot{\varepsilon}\right) = \frac{\partial \ln(m/(m+1))}{\partial \ln \dot{\varepsilon}} + m > 0 \qquad (5)$$

A superimposition of the efficiency of power dissipation and an instability maps for each deformed material is desired. Figure 12 represents processing and instability contour map for temperature range from 200 ˚C to 450 °C and strain rates 0.001 s^{-1} to 10 s^{-1} at strain 0.4. The instable zone with $\xi < 0$ appears in the temperature ranges between 200 °C - 250 °C and 400 - 450 °C at higher and lower strain rates. Also lower values for efficiency of power dissipation in above mentioned temperature regions (200 - 250 °C and 400 - 450 °C) and entire strain rates regions indicate the microstructurale changes that can result in cracking. Areas with lower values of efficiency of power dissipation are on lower and upper temperature regions for all tested strain rates. Mentioned lower values for efficiency of power dissipation indicate that larger part of energy is transferred in heat and smaller part in microstructure changes; consequently it could indicate lower deformability.

On Figure 13a the macroscopic view of occurrence of cracks on the surface of the specimen deformed at strain rate of 10 s^{-1} and temperature of 450 °C is presented. Mentioned cracks are consequence of precipitated (α_{Mg} + $Al_{12}Mg_{17}$) eutectic (melting point 426 °C, Figures 3 - 6) on grain boundaries (Figures 13b-d). Since the mentioned eutectic is at 450 °C in liquid state and due to relative motion on grain boundaries during hot forming process it results in micro-cracking. At compression on 450 °C the cracks occur at all strain rates with exception at lowest (0.001s^{-1}, Figures 14). On Figure 14a is thus macro view of surface of deformed specimen, on Figure 14b microstructure of larger area of deformed specimen and on Figures 14c-d the recrystallized grains are presented. The presence of dynamic recrystallization namely hinder the cracks growth as a consequence of (α_{Mg} + $Al_{12}Mg_{17}$) eutectic on grain boundaries.

The compression on temperature 400 °C and strain rates 5 in 10 s^{-1} also results in macro-cracks (Figure 15a) and micro-cracks (Figure 15b). These are consequence of precipitation of mentioned (α_{Mg} + $Al_{12}Mg_{17}$) eutectic and $Al_{12}Mg_{17}$ inter-metallic phase on grain boundaries (Figures 15c-d).

At lower strain rates the process of crack growth is hindered by the process of dynamic recrystallization; on Figure 16a the macro-view of deformed specimen at 400 °C and strain rate of 1 s^{-1}, on Figure 16b the microstructure of larger area of deformed specimen and on Figure 16c-d the presence of dynamic recrystallization is presented.

In the lower temperature region (200 – 250 °C) the hot forming is not possible since at higher

(10 and 5 s^{-1}) and also at lower strain rates (1, 0.01 and 0.001s^{-1}, Figure 17) macro-cracks occur (flow localisation bands, angle to compression axis is cca 45°). The mean reason was above mentioned ($\alpha_{Mg} + Al_{12}Mg_{17}$) eutectic and $Al_{12}Mg_{17}$ inter-metallic phase.

On Figure 18a macroscopic view of deformed specimen at 300 °C and strain rate of 1s^{-1} is shown. Its surface and its microstructure (Figure 18b) is error free. The same results at temperature 300 °C were also obtained for higher strain rates, i.e. 5 s^{-1} and 10 s^{-1}.

Areas with lower values of efficiency of power dissipation $\eta < 0.2$ (see Figure 12) are in very good accordance with obtained behavior of the alloy during its hot compression, i.e. in this area (at lower temperatures) micro-cracking occurred due to absence of dynamic recovery and dynamic recrystallization.

On the Figure 12 is thus denoted the areas where during hot compression cracks occurred and also the area (hatched) for safe hot forming.

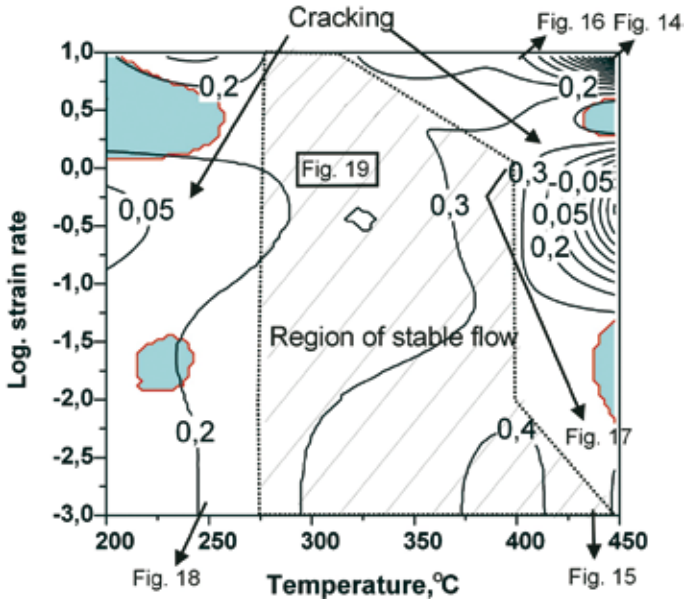

Figure 12. Superimposition of power dissipation map and instability map for temperature range from 200 ˚C to 450 ˚C, strain rates 0.001 s^{-1} to 10 s^{-1} and at strain 0.4

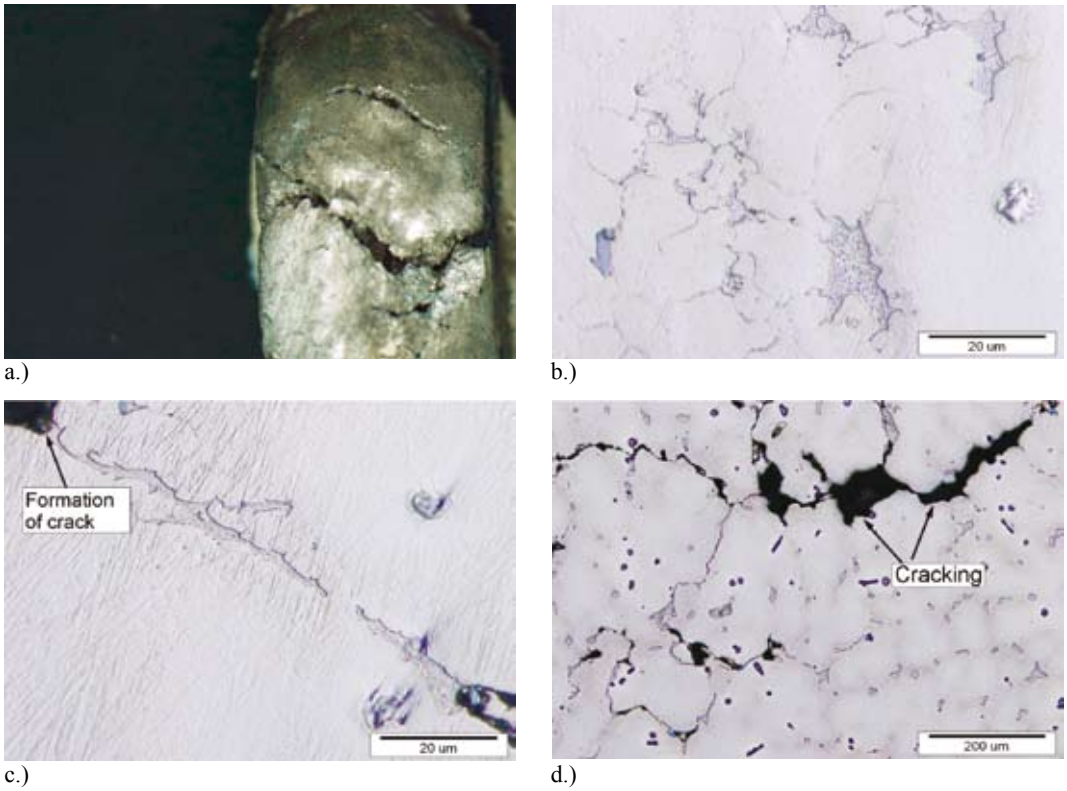

Figure 13. a-macroscopic view of deformed specimen, b-precipitations of (α_{Mg} + $Al_{12}Mg_{17}$) eutectic on grain boundaries, c-begin of crack formation on grain boundary with (α_{Mg} + $Al_{12}Mg_{17}$) eutectic, d-grain boundary cracking, deformation conditions: strain rate = $10s^{-1}$, temperature =450 °C

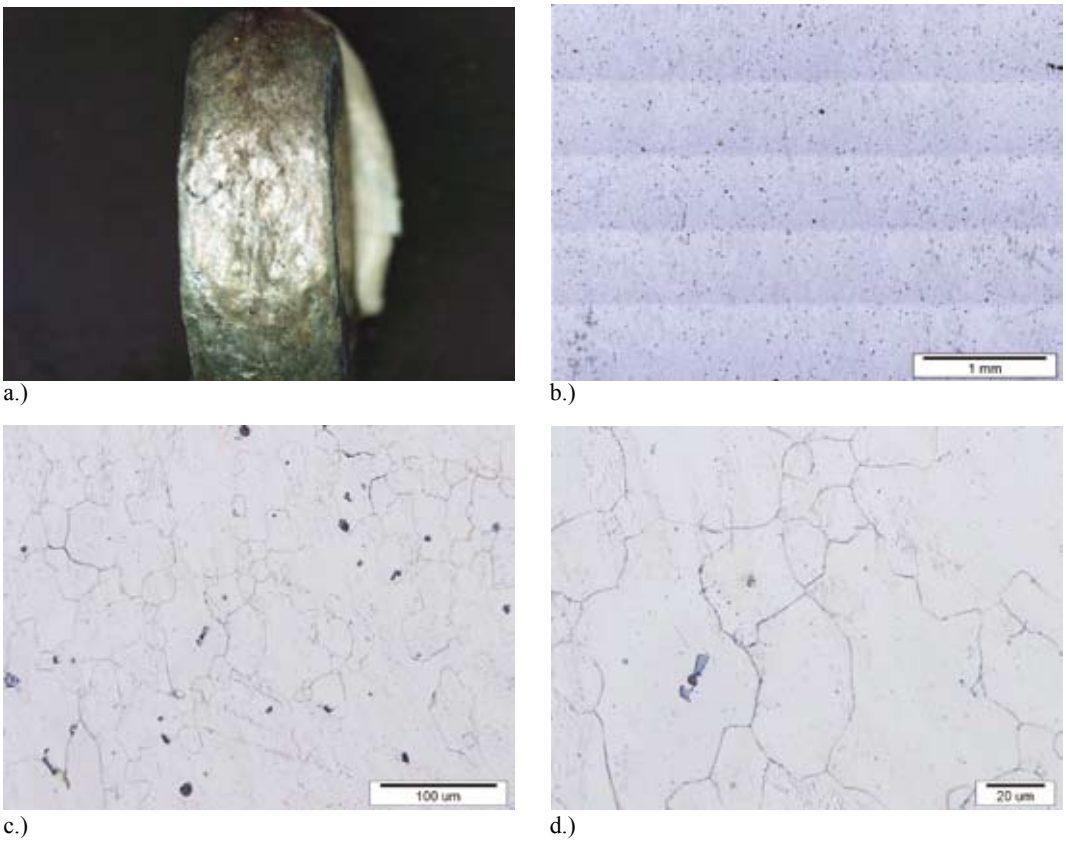

a.) b.)

c.) d.)

Figure 14. a-macroscopic view of deformed specimen, **b-**microstructure of larger deformed area, **c-d-**error free microstructure (recrystallization), deformation conditions: strain rate=0.001 s^{-1}, temperature =450 °C

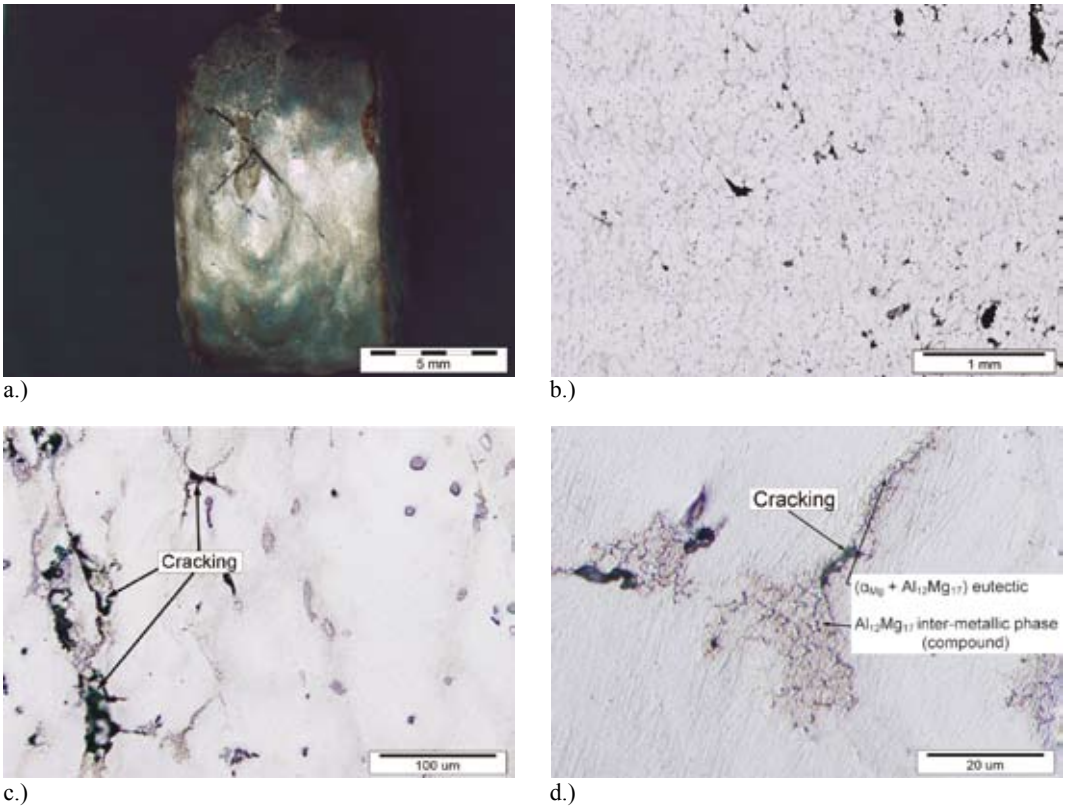

Figure 15. a-macroscopic view of deformed specimen, **b-**microstructure of larger deformed area, **c-d-**grain boundary cracking, and deformation conditions: strain rates = 5 - 10 s^{-1}, temperature =400 °C

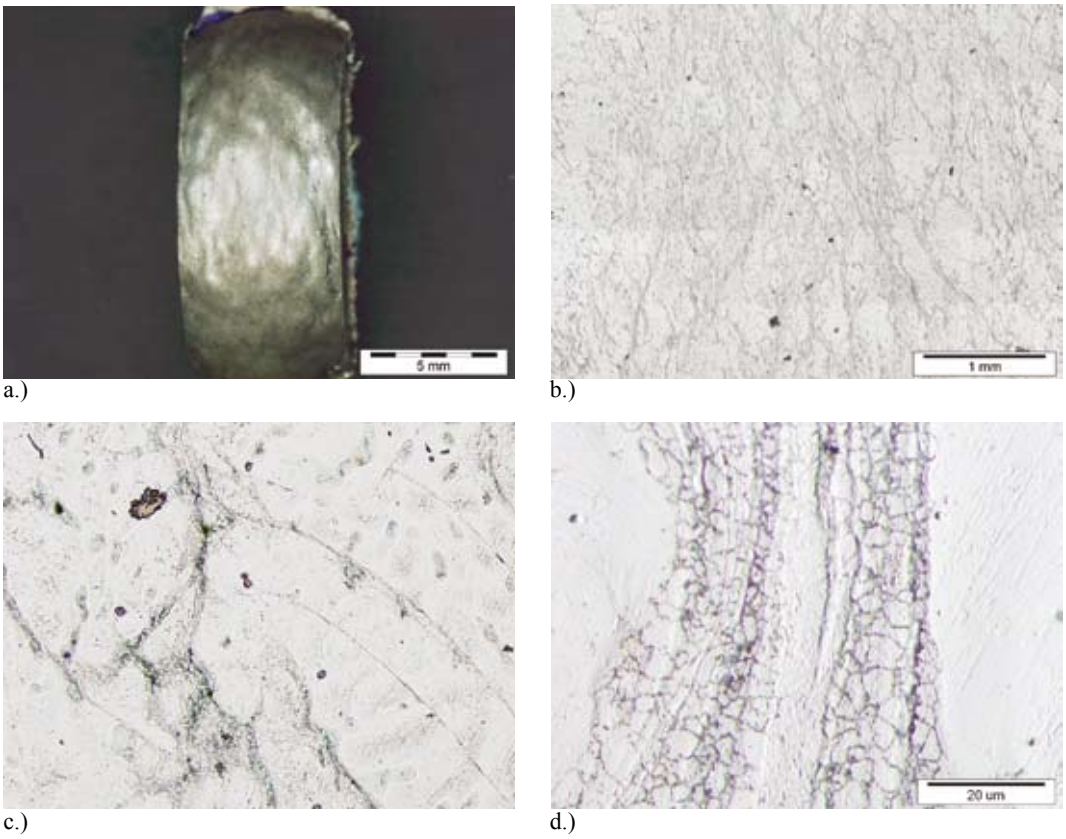

a.) b.)

c.) d.)

Figure 16. a-macroscopic view of deformed specimen, **b-**microstructure of large deformed area, **c-d-**error free microstructure (recrystallization on grain boundaries), deformation conditions: strain rate =1 s^{-1}, temperature =400 °C

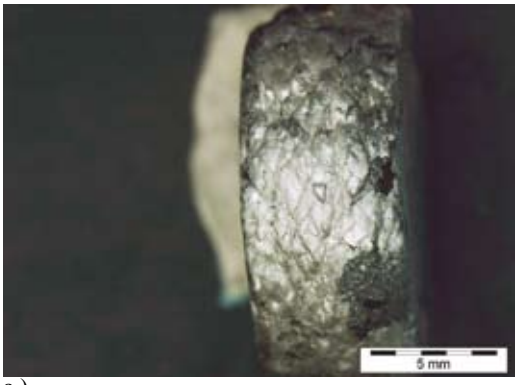

a.)

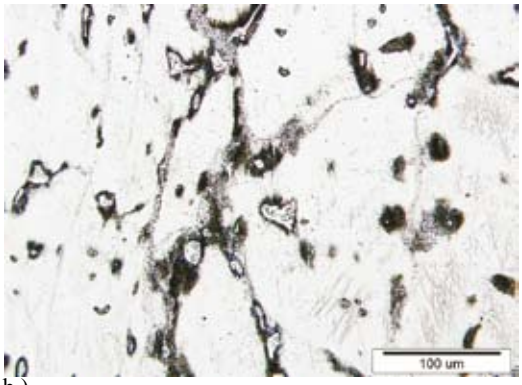

b.)

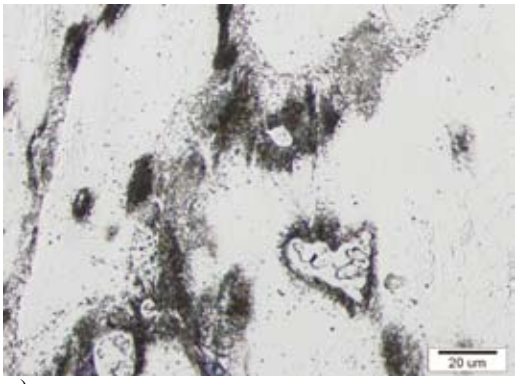

c.)

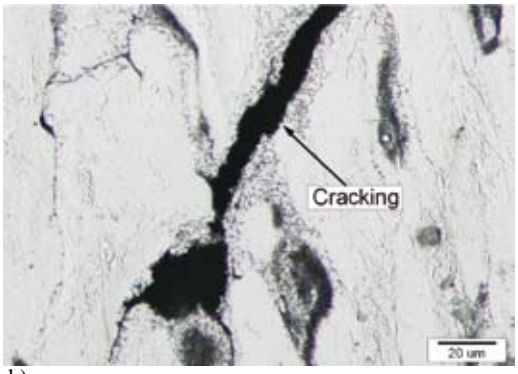

d.)

Figure 17. a-macroscopic view of deformed specimen, **b-c-**precipitation of ($\alpha_{Mg} + Al_{12}Mg_{17}$) eutectic and $Al_{12}Mg_{17}$ inter-metallic phase on grain boundaries, **d-**cracking on grain boundaries, deformation conditions: strain rate=0.001 s^{-1}, temperature = 250 °C

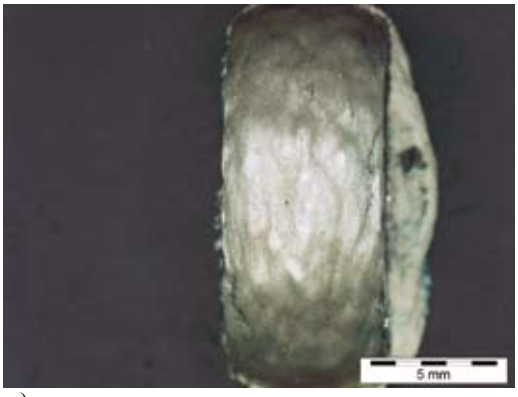

a.)

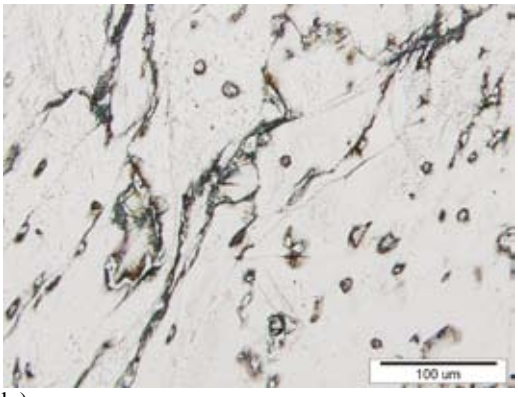

b.)

Figure 18. a-macroscopic view of deformed specimen, **b-**error free microstructure of deformed specimen, deformation conditions: strain rate =1s^{-1}, temperature =300 °C

CONCLUSIONS

From the cooling curves the solidification of the Mg-Al alloys was observed. The STA results show the accordance of the solidification course with the cooling curves. At the alloy AM60 the additional solidification peak was observed from the STA curves. That phenomena was connected by the eutectic crystallization, where the residual melt was transformed into the eutectic (α_{Mg} + $Al_{12}Mg_{17}$), which was established by the thermodynamic calculation and by the optical microscopy.

Due to the presence of manganese in the AM60 alloy the formation of the inter-metallic compound Al_4Mn is taking place with decreasing concentration of the dissolved aluminium in the molten metal, but the formation of eutectic (α_{Mg} + $Al_{12}Mg_{17}$) occurred at low cooling rate. The deformation characteristic of gravity as-cast MgAl6Mn alloy in the temperature range 200-450 °C and in the strain rate range 0.001-10 s^{-1} has been studied using processing maps. The following conclusions can be from mentioned investigation:

1. The alloy exhibit DRV and DRX in medium temperature range (300-400 °C) and at lower strain rates (0.001-1s^{-1}). Thus hot deformation can be performed in mentioned temperature and strain rates regions.
2. At temperatures higher than 426 °C the material exhibit lower ductility due to melting of (α_{Mg} + $Al_{12}Mg_{17}$) eutectic which is located on a grain boundaries.
3. At temperatures 250 °C and lower than the grain boundary cracking on grain boundaries due to precipitates of $Al_{12}Mg_{17}$ inter-metallic phase and (α_{Mg} + $Al_{12}Mg_{17}$) eutectic.
4. From technological (production) point of view the optimal temperature for hot forming is at 300 °C where the higher strain rates (5-10 s^{-1}) could be applied.

REFERENCES

[1] T.B. MASSALSKI, H. OKAMOTO: Binary Alloys Phase Diagrams 2nd ed. L. Subramanian, Kaprzak eds., ASM, Metal Park, Ohio, (1990).

[2] J. MEDVED, P. MRVAR: Thermal analysis of the Mg-Al alloys. Mater. sci. forum, 2006, let. 508, zv. 2, 603-608

[3] P. MRVAR, J. MEDVED, M. TRBIZAN, A. PAPEŽ, J. RAMOVŽ: Nonmetallic inclusions and intermetalic compounds in alloy AM60. Livar. vestn., 2005, let. 52, zv. 4, 146-159

[4] C.M. SELLARS, W.J. MCG. TEGART, La relation entre la resistance et la structure dans la deformation a chaud, Mem. Sci. Rev. Metal., 63 (1966), 731-746

[5] C.M. SELLARS, W.J. MCG. TEGART, Int. Metall. Rev., 17 (1972), 1-24

[6] J.J. JONAS, C.M. SELLARS, W.J. MCG. TEGART, Metall. Rev., 130 (1969), 1-24

[7] G.KUGLER, M.KNAP, H.PALKOVSKI AND R.TURK, Estimation of activation energy for calculating the hot workability properties of metals, Metalurgia, 43/4 (2004) 267-272.

[8] Y.V.R.K. PRASAD, S. SASIDHARA, Hot Working Guide, A Compendium of Processing Maps, ISBN: 0-87170-589-2, ASM International 1997.